The Structure of Nitromalonamide: A Combined Neutron-Diffraction and Computational Study of a Very Short Hydrogen Bond

Georg K. H. Madsen,[†] Claire Wilson,[†,‡] Thomas M. Nymand,[†] Garry J. McIntyre,[§] and Finn K. Larsen*,[†]

Department of Chemistry, University of Aarhus, DK-8000 Århus C., and Institut Laue-Langevin, BP 156, 38042 Grenoble Cedex 9, France

Received: March 30, 1999; In Final Form: August 26, 1999

Nitromalonamide has a remarkably short intramolecular hydrogen bond with an O−O distance of 2.391(3) Å, which according to some expectations would indicate a symmetric hydrogen bond. However, the enol hydrogen is confirmed by neutron diffraction to have an asymmetric position between the two oxygen atoms in the otherwise quite symmetrical molecule. The O−H distances are 1.14(1) Å and 1.31(1) Å. Analysis of the atomic displacement parameters of the enol hydrogen and comparison with those of similar systems indicate that the hydrogen atom resides in a single well potential. The experimental structure is compared to geometry optimized structures obtained from high level ab initio computations and, except for the position of the enol hydrogen, generally good agreement is obtained when correlation is taken into account. The significant differences between experimental and ab initio O−H bond lengths are ascribed to dynamical and intermolecular effects. Extremely small proton transfer barriers of 0.6 kJ/mol at the MP2/cc-pVTZ and 1.2 kJ/mol at the B3LYP/cc-pVTZ levels of theory were calculated. The enol hydrogen is found to vibrate freely between the two oxygen atoms, without the molecule passing through a well refined transition state structure. A simple model of the crystal environment explains the asymmetry of the hydrogen bond as resulting from intermolecular hydrogen bonding.

Introduction

Hydrogen bonds hold much fascination, and some of the most interesting are the short strong ones.[1,2] Following Hibbert and Emsley,[2] hydrogen bonds can be classified into three categories: weak (normal) hydrogen bonds, in which the proton is confined to the potential well near one atom, strong low barrier hydrogen bonds (LBHB), in which the zero-point vibrational energy (ZPVE) of the hydrogen (but not of deuterium) exceeds the proton transfer barrier, and finally very strong hydrogen bonds, in which both hydrogen and deuterium atoms have sufficient ZPVE to shuttle between the two hydrogen-bonded atoms. Strong O−H··O hydrogen bonds are believed to exist when the O−O distance is shorter than 2.5 Å. Further decrease of the O−O distance is accompanied by a lengthening of the O−H bond and a shortening of the O··H bond until a symmetrical hydrogen bond may be reached for $d_{O-O} \approx 2.39-2.40$ Å. (See for example Figure 3.5 in ref 1and Figure 1 in ref 2.) The study of strong hydrogen bonds is an area of active research. They have lately been shown to exist in a high-pressure phase of ice[3] and have been suggested to play a role in enzyme catalysis.[4] At least one enzyme, scytalone dehydratase, is known to involve the keto−enol form of a β-diketone.[5] We have recently reported the first very-low-temperature combined neutron and X-ray diffraction study of a LBHB in a keto−enol (benzoylacetone).[6] In the present study we describe the structure of nitromalonamide as a further example of a detailed study of a very short intramolecular O−H−O hydrogen bond in a keto−enol system.

While most strong hydrogen bonds involve charged fragments, keto−enoles constitute an intriguing set of compounds that form strong intra- and intermolecular hydrogen bonds in which nominally no charges are involved.[7] To rationalize the short hydrogen bonds in these conjugated neutral systems, Gilli et al. have proposed the resonance assisted hydrogen bonding (RAHB) model, according to which the strength of the hydrogen bond is linked to the resonance in the keto−enol system.[8]

Keto−enol compounds in some cases exhibit disorder−order phase transitions,[9] and it can be argued that the crystal structures of keto−enol compounds can be determined reliably only by low-temperature neutron diffraction. In the low-temperature neutron-diffraction study of benzoylacetone it was demonstrated that the structure is ordered with the enol hydrogen located close to the midpoint between the two oxygen atoms, but exhibiting a very large root-mean-square vibrational amplitude along the O−O vector.[6] Furthermore some fourth-order anharmonic displacement parameters of the enol−hydrogen were found to be significant. This was interpreted to mean that the hydrogen has sufficient energy to shuttle between the two oxygen atoms in a low-barrier potential well. By combined analysis of X-ray and neutron-diffraction measurements an experimental electron density was derived.[6] A topological analysis of the electron density revealed considerable charge localization in the hydrogen bond and indicated that the bonding has both electrostatic and covalent character. The results lead to a modification of the RAHB model originally proposed by Gilli and co-workers to account for the short hydrogen bonds observed in keto−enol systems.

* Corresponding author. E-mail: kre@kemi.aau.dk. Fax: (+45) 8619 6199.

[†] University of Aarhus.

[‡] Present address: Department of Chemistry, University of Durham, Durham DH1 3LE, England.

[§] Institut Laue-Langevin.

10.1021/jp991102i CCC: $18.00
Published on Web 10/12/1999

The crystal structure of nitromalonamide was determined at room temperature using X-ray diffraction, and it exhibits one of the shortest intramolecular hydrogen bonds found in keto−enol systems.[10] The present paper presents the structure of nitromalonamide studied by low-temperature neutron diffraction. In an attempt to evaluate the influence of the intermolecular hydrogen bonding on the keto−enol ring and to evaluate the proton-transfer barrier, our experimental results will be compared with high level ab initio computations.

Experimental Section

Neutron Diffraction Study. Single crystals were grown by evaporation from a methoxy−ethanol solution. A box-shaped crystal was mounted on an aluminum pin using Araldite epoxy resin and wrapped in a strip of aluminum foil. It was then placed in a Displex cryo-refrigerator and cooled to and maintained at 15 ± 0.5 K while the neutron diffraction data were collected using monochromatic thermal neutrons with a wavelength of 0.955 Å on D19, a four-circle neutron diffractometer on the H11 thermal beam at the Institut Laue-Langevin, Grenoble. This diffractometer is equipped with a 64 × 4° vertically curved two-dimensional position-sensitive detector which allowed the data to be collected reasonably efficiently in normal-beam Weissenberg geometry. The observed three-dimensional count distribution around each reciprocal lattice point was corrected for background and reduced to an integrated intensity I by a method that minimizes the relative standard deviation, $\sigma(I)/I$.[12] The Lorentz correction appropriate to normal-beam geometry was also applied. Further experimental details are given in Table 1. An initial check of the crystal quality before cooling revealed some extra peaks, indicating the presence of one or more parasite crystals. The strongest of the extra reflections could be indexed and attributed to an additional crystallite with 1.5% of the volume of the main crystal, rotated 3.1° around the [0 1 0] direct axis. Strong reflections from the additional crystal affected the integration of some of the weak reflections of the main crystal, which was manifested principally by a large mismatch between the predicted and observed centroids of the local three-dimensional count distribution. These reflections were omitted from further analysis. The 4043 data unaffected by the parasite crystal were corrected for absorption by Gaussian integration and averaged over symmetry equivalents.

A structural model, including anisotropic thermal parameters on all atoms, was fitted to the experimental data by a full-matrix least-squares refinement carried out with the program XD.[12] Although thermal motion is minimized at 15 K, bond-length corrections for libration of hydrogen atoms can still be significant and necessary for comparisons with high-level theoretical calculations.[13] Corrections to the N−H bond lengths can be calculated from the anisotropic displacement factors.[14] However, a more direct method is to include anharmonic parameters in the displacement factor.[15] Including a third-order Gram−Charlier expansion[16,17] the displacement factor is written as

$$T(\mathbf{H}) = T_0(\mathbf{H})\left(1 - \frac{4}{3}\pi^3 i \sum_{jkl} c^{jkl} h_j h_k h_l\right) \qquad (1)$$

where $T_0(\mathbf{H})$ is the anisotropic (harmonic) displacement factor, c^{jkl} the anharmonic third-order coefficients, and h_i the ith element of the scattering vector **H**. Refinement of a model including such anharmonic displacement factors for all hydrogen atoms led to an improvement of the reliability factor and some third-order parameters refined to values significant at the 2σ level.

TABLE 1: Experimental Details

crystal data	neutron study
formula	$C_3N_3O_4H_5$
formula weight	147.0902
space group	orthorhombic P $2_12_12_1$
a (Å)	4.842(2)
b (Å)	4.967(2)
c (Å)	21.899(7)
V (Å^3)	526.7(3)
Z	4
D_x (Mg m^{-3})	1.847
radiation	neutron
wavelength (Å)	0.9545(5)
no. reflections for cell	3256
θ range for cell reflections	5.7−59.2
μ (mm^{-1})	0.158
temp (K)	15.0(5)
cryst morphology	colorless crystal bounded by ±[001] 1.5 mm, ±[102] 3.5 mm, ±[−102] 3.5 mm, ±[011] 3.3 mm, ±[0−11] 3.3 mm
data collection	
diffractometer	D19 at the ILL
scan method	normal beam Weissenberg
trans factors	0.5905−0.7865
no. measured reflections	4043
no. unique reflections	1460
R_I	4.17%
range h,k,l	$h = -8,8$; $k = -8,8$; $l = -17,38$
no. standards	6
freq of standards	every 100 reflections
intensity decay (%)	none
refinement on	F^2
R(F), R(F^2) (%)	5.71, 8.71
wR(F), wR(F^2) (%)	5.06, 9.62
GoF	1.677
N_{obs}, $I > 2\,\sigma(I)$	1342
N_{par}	186
$N_{obs/par}$	7.215
weighting scheme	$1/\sigma^2(F^2)$

Also, fourth-order anharmonic parameters were tested for the enol hydrogen, but none refined to significant values, and they were not included in the final model. Extinction was found to be insignificant, probably because of the parasite crystals and the resulting high mosaic spread. The final model was tested by refining against data above different $\sigma(F^2)/F^2$ cutoffs. The positional and atomic displacement parameters (ADPs) were essentially independent of the cutoff, and the reported model corresponds to a $2\sigma(F^2)/F^2$ cutoff criterion. According to Hirshfeld's rigid bond test,[18] the difference in mean-square displacement amplitude (MSDA) in the direction of the bond between two atoms, A and B, of similar mass, $\Delta\langle u^2\rangle_{A,B}$, should not exceed 10^{-3} Å^2 for a well-determined structure. Only one bond just exceeds Hirshfeld's limit, the N(2)−O(22) bond, which has $\Delta\langle u^2\rangle_{N(2),O(22)} = 0.0013(10)$ Å^2. Further experimental details and refinement residuals are given in Table 1. An ORTEP[19] plot of nitromalonamide is shown in Figure 1. Atomic positional and displacement parameters have been deposited as a CIF file in the Supporting Information.

Ab Initio Calculation Procedures. Quantum chemical ab initio calculations were carried out for nitromalonamide at three different levels of theory. Hartree−Fock (HF), Møller−Plesset second-order perturbation theory (MP2), and density functional theory (DFT) calculations were carried out with the *Gaussian 94* program.[20] In the DFT calculations, Becke's three parameter hybrid exchange functional (B3)[21] and the Lee−Yang−Parr (LYP)[22] correlation functional were used. In all calculations, the cc-pVXZ basis sets of Dunning[23] were used. HF calculations were carried out with the cc-pVDZ basis set, and the MP2 and

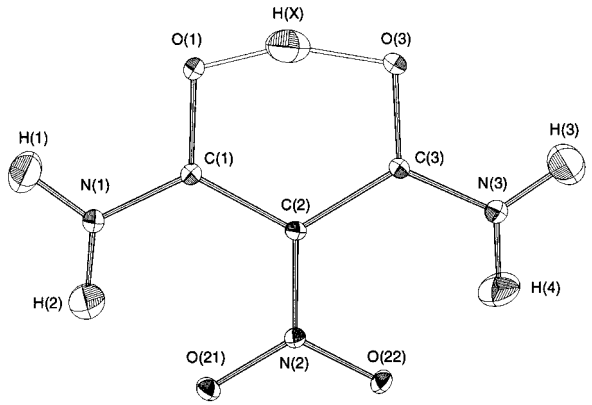

Figure 1. ORTEP drawing of nitromalonamide showing the atom numbering and 50% probability ellipsoids.

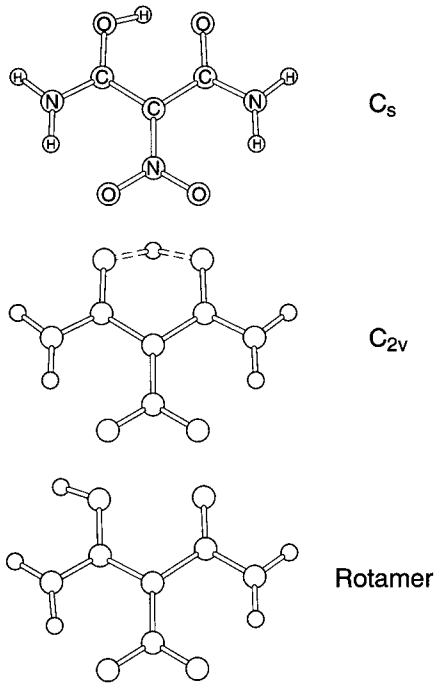

Figure 2. Structures of different symmetry used in the ab initio calculations on nitromalonamide.

B3LYP calculations with both the cc-pVDZ and cc-pVTZ basis sets. The numbers of basis functions used were 165 and 370 for the cc-pVDZ and cc-pVTZ sets, respectively. On the basis of the experimental structure, the molecule was constrained to be planar. Geometry optimizations were subsequently carried out at all levels of theory in the two different conformations in which an intramolecular hydrogen bond is formed. The proton involved in this bonding is either delocalized, in which case the molecule possesses C_{2v} symmetry, or localized in which case the symmetry is C_s, Figure 2. In both conformations, the point group symmetry was maintained during optimization. Further, geometry optimizations of the rotamer, which excludes the intramolecular hydrogen bond, were performed at the MP2/cc-pVDZ and B3LYP/cc-pVDZ levels, thus enabling us to estimate the hydrogen bond energy. Finally, frequencies were computed at the B3LYP/cc-pVDZ level of theory by a harmonic extrapolation of the energy surface around the optimized positions. Since the potential energy surface around the enol hydrogen is not expected to be harmonic, the energies of the normal modes involving the enol hydrogen atom should be taken with some caution. In the following they are mainly used for qualitative arguments. Also, complete active space calculations have been performed; however, the very limited description of correlation offered by the multiconfiguration self-consistent field method applied gave results that compare poorly with the experimental results. The discussion of the attempt has been deposited as Supporting Information.

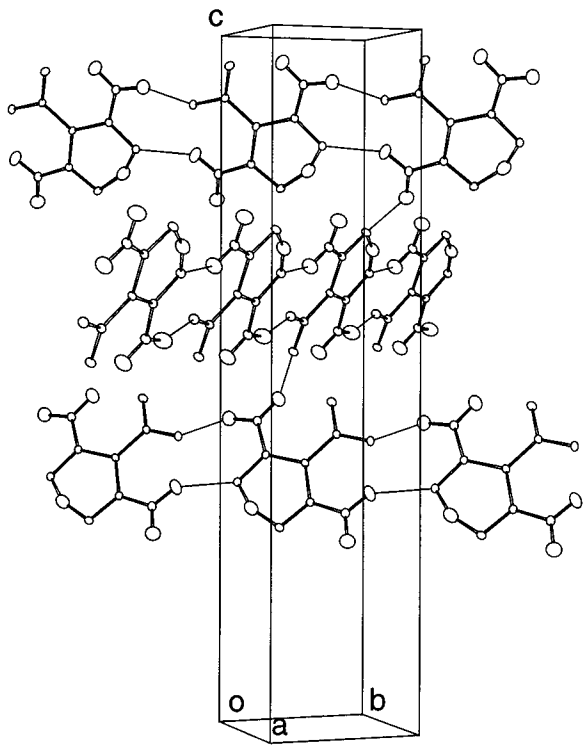

Figure 3. ORTEP drawing of the structure. Ribbons of hydrogen bonded molecules in neighboring layers are shown. The intermolecular hydrogen bonds are shown with thin lines.

Results and Discussion

Experimentally Determined Structure. The crystal structure of nitromalonamide is characterized by extended three-dimensional hydrogen bonding. Ribbons of almost coplanar molecules are formed through intermolecular N−H···O hydrogen bonding [N(3)−H(4)···O(1) and N(1)−H(1)···O(22)]. The ribbons form layers parallel to the *ab* plane with no interribbon hydrogen bonds within the layer. The layers stack along the *c*-axis, and neighboring layers have the ribbons running in orthogonal directions, Figure 3. The layers are connected with intermolecular hydrogen bonds [N(3)−H(3)···O(3) and N(1)−H(2)···O(21)].

The bond lengths and bond angles for nitromalonamide are given in Table 2 and Table 3. Most remarkable is the short intramolecular hydrogen bond, O(1)−O(3) of length 2.391(3) Å. The intramolecular hydrogen bonding significantly lengthens the O(1)−H(X) bond compared to a normal covalent O−H bond. This important fact was not noted in the much less precise room-temperature X-ray structure, where O(1)−H(X) was determined to be 1.01 Å.[10] Nevertheless, the enol hydrogen refines to a position that is significantly asymmetric, with the O(1)−H(X) distance of 1.140(10) Å being 16 standard uncertainties shorter than the O(3)−H(X) distance of 1.308(11) Å. This is somewhat contrary to expectations as crystal structure correlations have been reported showing that a decrease of the O−O distance is accompanied by a lengthening of the O−H bond and a shortening of the O··H bond until a symmetrical hydrogen bond may be reached for $d_{O-O} \approx 2.39-2.40$ Å.[1,2]

TABLE 2: Interatomic Distances and Angles

bond	Å	angle	deg
O(1)−O(3)	2.391(3)	O(1)−H(X)−O(3)	155.1(8)
O(1)−H(X)	1.140(10)	C(1)−O(1)−H(X)	105.9(5)
O(3)−H(X)	1.308(11)	C(3)−O(3)−H(X)	104.7(5)
O(1)−C(1)	1.292(3)	O(1)−C(1)−C(2)	117.8(2)
O(3)−C(3)	1.285(3)	O(1)−C(1)−N(1)	117.7(2)
O(21)−N(2)	1.256(2)	C(2)−C(1)−N(1)	124.4(2)
O(22)−N(2)	1.258(3)	C(1)−C(2)−C(3)	118.7(2)
C(1)−C(2)	1.466(3)	C(1)−C(2)−N(2)	120.2(2)
C(2)−C(3)	1.463(2)	C(3)−C(2)−N(2)	121.0(2)
C(1)−N(1)	1.317(2)	O(3)−C(3)−C(2)	117.7(2)
C(2)−N(2)	1.394(2)	O(3)−C(3)−N(3)	118.9(2)
C(3)−N(3)	1.323(2)	C(2)−C(3)−N(3)	123.3(2)
N(1)−H(1)	1.011(10)	C(1)−N(1)−H(1)	116.1(6)
N(1)−H(2)	1.021(9)	C(1)−N(1)−H(2)	121.5(6)
N(3)−H(3)	1.026(9)	H(1)−N(1)−H(2)	122.3(8)
N(3)−H(4)	1.025(9)	O(21)−N(2)−O(22)	120.0(2)
O(21)···H(2)	1.897(11)	O(21)−N(2)−C(2)	120.0(2)
O(22)···H(4)	1.851(10)	O(22)−N(2)−C(2)	119.9(2)
		C(3)−N(3)−H(3)	120.1(6)
		C(3)−N(3)−H(4)	119.4(7)
		H(3)−N(3)−H(4)	120.5(9)
		N(2)−O(21)··H(2)	111.3(3)
		N(2)−O(22)··H(4)	110.3(3)
		N(1)−H(2)···O(21)	122.3(7)
		N(3)−H(4)···O(22)	125.8(8)

TABLE 3: Intermolecular Distances and Angles[a,b]

bond	Å	angle	deg
O(1)···H(4)#1	2.278(11)	C(1)−O(1)···H(4)#1	131.2(3)
O(3)···H(3)#2	2.053(11)	C(3)−O(3)···H(3)#2	119.5(4)
O(21)···H(2)#3	2.118(9)	N(2)−O(21)···H(2)#3	107.3(3)
O(22)···H(1)#4	1.920(10)	N(2)−O(22)···H(1)#4	151.9(3)
		N(3)−H(4)···O(1)#4	137.0(8)
		N(1)−H(1)···O(22)#1	159.5(7)
		N(1)−H(2)···O(21)#5	141.7(8)
		N(3)−H(3)···O(3)#6	142.6(8)

[a] Accurate cell constants (a = 4.862(1) Å, b = 4.980(1) Å, c = 21.938(5) Å) obtained from a single-crystal X-ray study at 10 K were used for calculation of the bond lengths. [b] Symmetry transformations used to generate equivalent atoms: #1, $-1+x, 1+y,z$;#2, $2-x$, 1/2 + y, 3/2 − z; #3, 1/2 + x, −1/2 − y, 1 − z; #4, 1 + x, −1 + y,z ; #5, −1/2 + x, −1/2 − y, 1-z #6, 2 − x, −1/2 + y, 3/2 − z.

The oxygen atoms of the nitro group seem to be part of intra- as well as intermolecular N−H···O hydrogen bonds. The molecule sits in an asymmetric crystal environment where O(1) accepts a nearly in-plane intermolecular hydrogen bond from H(4)#1 while the intermolecular hydrogen bond O(3)···H(3) shows a torsion angle of 30.8° for C(2)−C(3)−O(3)···H(3)#2. The two C−C bond lengths do not differ significantly, and the two C−O bond lengths differ by just two standard uncertainties with the C(1)−O(1) bond being slightly longer than the C(3)−O(3) bond. The two C−N amide bonds, however, are barely significantly different, with C(1)−N(1) being shorter than C(3)−N(3). In other words, O(3)−C(3)−N(3) has more amide character than O(1)−C(1)−N(1), in accordance with the asymmetric position of H(X). All C−C, C−O, and C−N bonds lie between the average values for double and single bonds,[24] indicating that the π-conjugation extends over the entire molecule. Both C−C bonds are significantly longer than the corresponding bonds in the benzoylacetone molecule,[6] thus indicating that the conjugation to the amino groups influences the C−C conjugation. The symmetry coordinate Q defined as $Q = d_{C(1)-O(1)} + d_{C(2)-C(3)} - (d_{C(1)-C(2)} + d_{C(3)-O(3)})$ (ref 8) gives a concise description for the amount of delocalization in the enol ring. For nitromalonamide the value Q = 0.004 Å indicates a very symmetric, delocalized enol ring. As a result of the extended π-conjugation and the three intramolecular hydrogen bonds, the nitromalonamide molecule is almost planar, the largest intramolecular torsion angle being between C(2)−C(1) and N(1)−H(2) of 3.1°.

TABLE 4: Comparison of the MSDA of the Enol Hydrogen along the O−O Vector for Short Hydrogen Bonds

molecule	ref	temp (K)	d_{O-O} (Å)	d_{O-H} (Å)	d_{O-H} (Å)	$\langle u^2\rangle_{O-O}$ (Å^2)
benzoylacetone	30	300	2.489(5)	1.235(11)	1.319(12)	0.174
benzoylacetone	6	20	2.502(4)	1.245(11)	1.329(11)	0.106
nitromalonamide		15	2.391(3)	1.140(10)	1.308(11)	0.031
DQNA	25	35	2.398(3)	1.150	1.252	0.018
	25	100	2.398(3)	1.150	1.252	0.023
MAHS	26	110	2.442	1.221	1.221	0.026
MADMA	27	122	2.419	1.213	1.213	0.025
	27	122	2.415	1.210	1.210	0.032
ClMH	28	100	2.383(4)	1.149(7)	1.235(7)	0.022

The curvilinear motion of the amide hydrogens was modeled by including anharmonic parameters in the displacement factor. Generally the inclusion of the third-order parameters on the amide hydrogen atoms led to N−H bond lengths which are up to 0.018 Å longer than values determined with the harmonic model. Inclusion of third-order parameters on the enol hydrogen shortens the O(1)−H(X) bond by 0.003 Å and diminishes the O(1)−H(X)−O(3) bond angle by 1.5 °.

Thermal motion of the enol hydrogen. The ADPs of the enol hydrogen determined from the neutron data supply information about the nature of the enol potential well. Comparison of ADPs from our studies of benzoylacetone and nitromalonamide with literature values from other neutron diffraction studies of compounds with very short O−H−O hydrogen bonds is hampered by the fact that the O−H−O bonds are not all quite linear. In an attempt to put the MSDA values on a common ground we have calculated the MSDA along the O−O vector of the hydrogen atoms, $MSDA_{O-O}$, for the compounds compared in Table 4. The short O−H−O hydrogen bonds in deuterated quinolinic acid[25] (DQNA), methylammonium hydrogen succinate monohydrate[26] (MAHS), methylammomium hydrogen maleate[27] (MADMA), and 1,2-dicloromaleic acid[28] (ClMH) can be termed (−) charge assisted hydrogen bonds [(−)CAHB] in the nomenclature of Gilli et al.,[29] while benzoylacetone[6,30] and nitromalonamide are RAHB systems. Except for benzoylacetone, the compounds show quite similar $MSDA_{O-O}$ values ranging from 0.018 to 0.032 Å^2. The only study carried out at a temperature comparable to the keto−enol studies is of a deuterated sample DQNA. The same study also reports a comparison at 100 K of the MSDAs of deuterated (DQNA) and hydrogenated (HQNA) samples. It shows that the deuteration systematically lowers the MSDA by approximately 15%, and DQNA shows $MSDA_{O-O}$ totally in line with the results of the other 100 K studies. It is striking how benzoylacetone stands out from the crowd, while nitromalonamide has a $MSDA_{O-O}$ that is comparable to the values observed for all the other compounds with O−O distance close to 2.4 Å. We take this to indicate that despite differences in asymmetry the hydrogen sits in a similar type potential well for all the compounds listed in Table 4 except for benzoylacetone.

Ab Initio Structure. Table 5 gives an overview of the structural and energetic parameters obtained from the ab initio calculations. It is well known[31] that inclusion of correlation effects is mandatory when studying keto−enol systems with ab initio methods, and the HF results are mainly included here for the sake of completeness. In the following, the ab initio structure obtained from the descriptions including correlation

TABLE 5: Resume of Theoretical Results[a]

		C_s					C_{2v}			$E_{C_s} - E_{C_{2v}}$
method	basis set	energy	O−O	O−H	O−H	Q	energy	O−O	O−H	energy
HF	cc-pVDZ	−579.28427	2.426	0.993	1.510	0.108	−579.28060	2.310	1.177	9.63
MP2	cc-pVDZ	−580.91537	2.390	1.080	1.348	0.063	−580.91512	2.356	1.194	0.661
	cc-pVTZ	−581.48868	2.379	1.078	1.343	0.060	−581.48843	2.348	1.191	0.646
B3LYP	cc-pVDZ	−582.47476	2.384	1.095	1.335	0.052	−582.47464	2.358	1.199	0.310
	cc-pVTZ	−582.65659	2.394	1.065	1.382	0.069	−582.65616	2.350	1.197	1.123
exptl			2.391(3)	1.14(1)	1.31(1)	0.004				

[a] All distances are in Å. Total energies are in au. The barrier height estimated as the differences between C_s and C_{2v} energies is given in kJ/mol.

will be compared to the experimental structure to validate the level of theory employed.

In the MP2 treatment, the change of basis set from double-ζ to triple-ζ unequivocally shortens the optimized bond lengths, the decrease being between 0.002 and 0.015 Å. This result agrees well with the findings of a systematic study of bond lengths obtained from ab initio calculations.[32] The small changes indicate that our MP2/cc-pVTZ calculations yield bond lengths close to those at the basis set limit. If the O(1)−H(X) and O(3)−H(X) bonds are left out of the discussion, the largest differences between the experimental structure and the C_s MP2/cc-pVTZ structure are that the C(1)−C(2) bond length is estimated 0.037 Å too short and the N−H bond lengths are estimated between 0.007 and 0.022 Å too short. Lists of the molecular ab initio interatomic distances are given in the Supporting Information. The good agreement between the experimental and the ab initio results also holds for the B3LYP method. In this case, changing the basis set from double-ζ to triple-ζ generally shortens the bonds by at most 0.010 Å. Only one bond is lengthened (C(1)−O(1) by only 0.001 Å). The largest differences between the experimental structure and the C_s B3LYP/cc-pVTZ are that the C(1)−C(2) bond length is estimated 0.032 Å too short and the N−H bonds are estimated between 0.006 and 0.021 Å too short. Our present study confirms that hybrid HF/DFT methods provide an alternative to post-Hartree−Fock methods, such as MP2, and can provide quite accurate ground-state properties at a remarkably low cost.[33,34]

The agreement between experimental and ab initio values has some flaws and definitively does not hold when examining the all-important intramolecular O−H−O bond. Neither the MP2 nor the B3LYP methods correctly predict the substantial lengthening of the O(1)−H(X) bond and shortening of the H(X)−O(3) bond that results from the formation of the RAHB. The MP2 and B3LYP O−O distances show opposite behavior on changing the basis set, with the B3LYP/cc-pVTZ distance being in very close agreement with the experimental distance. An examination of the values of the Q symmetry coordinate also reveals that differences between the experimental and theoretical bond lengths are systematic and result in $Q_{MP2/cc-pVTZ}$ being 0.060 Å and $Q_{B3LYP/cc-pVTZ}$ being 0.069 Å, much larger than $Q_{exp} = 0.004$ Å. It conforms with the RAHB model that an underestimation of the O−H bond length is accompanied by an underestimation of the resonance in the keto−enol ring.

In light of the different hydrogen potential wells sketched in the Introduction, the disagreement between the experimental and ab initio structures around the O−H−O fragment is interesting. The good internal agreement between the structures obtained at the different levels of theory and otherwise good agreements between the ab initio and experimental structures mean that the explanation for the disagreements must rest in dynamical effects and perturbations of the crystal structure by intermolecular effects.

TABLE 6: Results of the Corrections For ZPVE at the B3LYP/cc-pVDZ Level of Theory[a]

	E_{C_s}	$E_{C_{2v}}$	$E_{C_s} - E_{C_{2v}}$
E_{elec}	−582.474758202	−582.474640082	−0.31
$E_{ZPVE,H}$	0.102921	0.101070	4.9
$E_{elec} + E_{ZPVE,H}$	−582.371838	−582.373570	4.5
$E_{ZPVE,D}$	0.089426	0.088277	3.0
$E_{elec} + E_{ZPVE,D}$	−582.282412	−582.285293	2.7

[a] Total electronic energies and ZPVE corrections (eq 2) are in au. The differences between C_s and C_{2v} energies and between rotamer and C_s energies are in kJ/mol.

Barrier Height And Proton Dynamics. When discussing dynamical effects it is important to appreciate what is actually observed in the diffraction experiment. As the interaction time of a neutron with the nuclear potential is several orders of magnitude shorter than the period of a lattice vibration, the diffraction experiment samples in space over many pseudostatic atomic configurations.[17] What we therefore observe are mean distances between the atoms. If the atomic potential is harmonic, the R_{mean} distances will be equal to the equilibrium distances R_e obtained from ab initio calculations. If, however, the potential energy surface around the hydrogen is very flat and asymmetric, this will not be the case. To investigate further the dynamical effects, the barrier height for proton transfer has been estimated by calculating the difference in total energy between the C_s structure and the C_{2v} transition state. Also, vibrational frequencies have been estimated through a harmonic extrapolation of the potential energy surface at the B3LYP/cc-pVDZ level of theory.

Both the MP2/cc-pVDZ and the MP2/cc-pVTZ give very low barrier heights of 0.662 and 0.642 kJ/mol, indicating that also the barrier height is close to the basis set limit estimate. The B3LYP method also predicts barrier heights that are extremely small, namely 0.310 kJ/mol (cc-pVDZ) and 1.123 kJ/mol (cc-pVTZ). To estimate the effective proton-transfer barrier, the energies must be corrected for the ZPVE, eq 2:

$$E_{ZPVE} = \frac{1}{2}\sum_{i}^{3N-6} \hbar\omega_i \qquad (2)$$

After the zero-point correction, the C_{2v} structure is found to be 4.5 kJ/mol more stable than the C_s structure, Table 6.

In the C_s structure, one normal mode with a reduced mass $\mu = 1.1631$ amu was identified to consist mainly of motion of the H(X) hydrogen atom. The frequency was found to be $\omega = 2011.6$ cm^{-1} which corresponds to a ZPVE of 12.0 kJ/mol. In the C_{2v} transition state structure, the E_{corr} summation runs over only $3N-7$ vibrational modes as there is one imaginary mode. The imaginary mode has a reduced mass of $\mu = 1.3229$ amu and mainly involves motion of the enol hydrogen. Note, however, that the C_{2v} structure is not simply stabilized by 12.0 kJ/mol, due to tightening of the remaining $3N-7$ modes in the

C_{2v} structure compared to the C_s structure. Therefore it is not a sufficient criterion for proton transfer to simply compare the ZPVE of a single mode with the electronic barrier heights in Table 5. ZPVE corrections were also calculated for nitromalonamide with a deuteron at the enol hydrogen position. Again the symmetric structure is found to be the most stable, Table 6, showing that the hydrogen potential well is effectively a single well potential.

Intermolecular Effects. The above considerations based on gas phase calculations imply that the hydrogen potential is effectively a symmetric single well potential and thus the average position of the hydrogen should be midway between the two oxygen atoms. In the experimental crystal structure, however, the enol hydrogen was observed to be located asymmetrically between the two oxygen atoms. To investigate the "in-crystal" electronic potential surface, a very crude model of the crystal environment was constructed. A central molecule was placed in the electrostatic potential arising from its two nearest neighbors in the hydrogen-bonded ribbons. The electrostatic potential of the two nearest neighbors was represented by a set of Mulliken charges at the atomic positions. Two calculations were performed at the B3LYP/cc-pVDZ level. One where the central molecule oriented as in the crystal structure and one where the central molecule is rotated 180° around the C(2)−N(2) direction. Thus, in the former O(1) receives an intermolecular hydrogen bond, and in the latter O(3) receives an intermolercular hydrogen bond. In both calculations the neighboring molecules maintained the C_s symmetry and their positions were determined by the experimental H(1)···O(22) and H(4)···O(1) hydrogen bonding distances given in Table 4. In this potential, the mirrored C_s structure has an energy that is 0.96 kJ/mol higher than the original C_s structure. Therefore, the potential energy surface is asymmetrical and consequently this simple model can qualitatively explain that the average position of the enol hydrogen lies closer to the O(1) oxygen atom acceptor of the in-plane intermolecular hydrogen bond.

Experimental Probability Density Function. In Figure 4, the experimental probability−density function (pdf) of the enol hydrogen is plotted together with the gas-phase potential-well models. When the displacement parameters are expanded up to third order, the resulting pdf is given as

$$\mathrm{pdf}(\mathbf{u}) = \mathrm{pdf}_0(\mathbf{u})\left(1 + \frac{1}{3!}\sum_{jkl} c_{jkl} H_{jkl}\right) \qquad (3)$$

where pdf_0 is the harmonic probability density function and H_{jkl} are the three-dimensional Hermite polynomials.[16,17] The curve in Figure 4 has been produced by calculating the probability of finding the enol hydrogen at points placed along the O(1)−H(X) and H(X)−O(3) bond vectors and provides a clear illustration of how the enol hydrogen moves freely between the two theoretical hydrogen positions. It is also important to note that the calculated O−O distance in the C_{2v} structure is more than 10 standard uncertainties shorter than the one observed experimentally. If the process occurred through a well-defined transition state, very large ADPs should be observed for the oxygen atoms, which is not the case. Therefore nitromalonamide does not seem to pass through a well-defined transition state, but instead the hydrogen moves freely between O(1) and O(3).

Proton transfer is a dynamical process and molecular dynamics (MD) simulations, such as the one performed recently on the proton-transfer process in malonaldehyde,[35] are interesting alternatives to traditional ab initio methods. In this study of malonaldehyde, the authors divided the proton transfer process into three parts: (i) normal periods where the proton is trapped on one oxygen, (ii) statistical isolated proton transfer transitions where the proton rapidly moves from one oxygen atom to the other, and, (iii) proton shuttling periods, which include several consecutive nonstatistical transitions. These are not true proton transfers. The proton is (quasi)-stationary within a (nearly) symmetric single-minimum potential which remains approximately constant for a longer period; the motion corresponds to a ν(OH) vibration with a frequency of about 2000 cm^{-1}. The average O−O distance at crossover points of proton-transfer transitions was found to be 2.38 Å. It is interesting how well the proton shutteling picture describes the situation in nitromalonamide. The difference between nitromalonamide and malonaldehyde is that in nitromalonamide the hydrogen stays in a single well potential where it vibrates freely between the two oxygens and no proton transfer occurs.

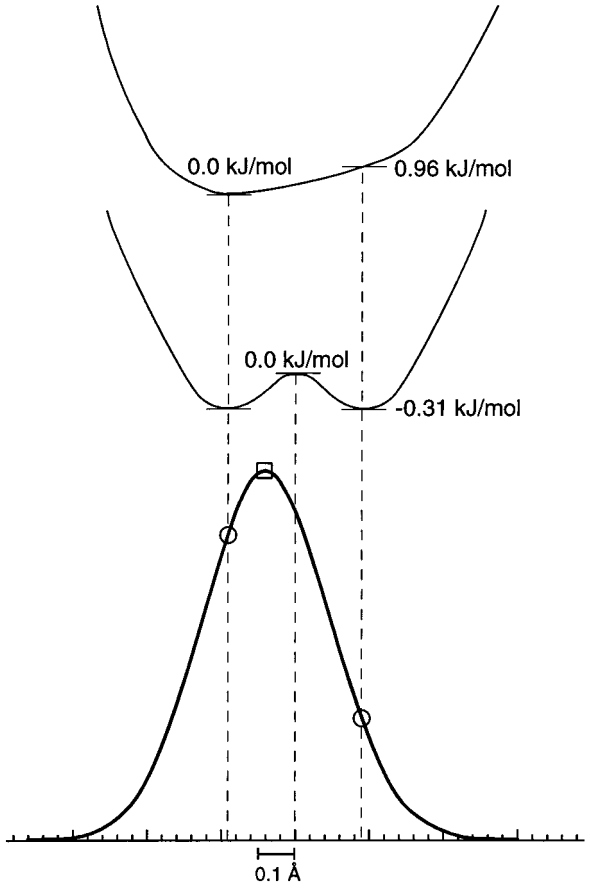

Figure 4. At the lower part of the figure is shown the experimental probability density function of H(X) along the O(1)−H(X)−O(3) bonds. The maximum defines the position of the enol hydrogen atom. In the upper part of the figure sketches of one-dimensional models of the enol hydrogen potential well are shown. The estimates of barrier heights are for the free molecule (middle) and an "in-crystal" molecule (top) and have been obtained at the B3LYP/cc-pVDZ level of theory.

One can view our experimental pdf of the enol hydrogen in nitromalonamide, Figure 4, as an experimental validation of the dynamical structures obtained from MD simulations of short hydrogen bonds.[3a,35]

Hydrogen Bond Strength. Finally, the strength of the intramolecular hydrogen bond has been estimated by comparing the energy of the C_s structure with a geometry optimized hypothetical rotamer structure. The difference between the hydrogen bonded structure and the rotamer structure was found to be 113.3 kJ/mol at the MP2/cc-pVDZ level and 116.3 kJ/mol at the B3LYP/cc-pVDZ level of theory. The MP2 and

B3LYP results are thus in very good agreement. The hydrogen bond energy is extremely high compared to a normal hydrogen bond energy (around 20 kJ/mol) and clearly falls within what Hibbert and Emsley define as a very strong hydrogen bond.[2]

Conclusions

The O−O distance of 2.391(3) Å found in nitromalonamide is one of the shortest observed in keto−enol systems and yet constitutes an asymmetric hydrogen bond. The present neutron diffraction study has shown that, in the solid state, the O(1)−H(X) bond is significantly longer than a normal O−H bond. However, the O(3)−H(X) bond is 16 standard uncertainties longer than the O(1)−H(X) bond. For comparison it should be mentioned that the enol hydrogen in benzoylacetone was found much closer to a central position, Table 4, even though the O−O distance is much longer.

All of the ab initio methods tested predict significantly less elongation of the O−H distance in the intramolecular O−H−O bond than found experimentally, while good agreement was obtained between the rest of the experimental structure and the MP2 and B3LYP when sorrelation is taken into account. When including dynamical effects into the calculation a symmetric hydrogen bond was predicted. The asymmetric position of the hydrogen has been explained to be a result of intermolecular hydrogen bonding. The energy difference between a symmetric structure and a structure with asymmetrically localized hydrogen was found to be extremely small, around 1 kJ/mol, which makes it understandable that especially the structure of the O−H−O region can be perturbed by intermolecular hydrogen bonding.

The MSDA of the enol hydrogen parallel to the O−O vector has been analyzed and compared to values of other short hydrogen bonds. The magnitude of the $MSDA_{O-O}$ in nitromalonamide was found to lie close to magnitudes observed experimentally for other similar systems with O−O distances around 2.4 Å, but far from what was observed for the LBHB in benzoylacetone.[6] A probability density function for the enol hydrogen has been calculated from the experimental data. This has shown that there is a large probability of finding the enol hydrogen also close to O(3), despite the asymmetric average position of the hydrogen which is close to O(1). Furthermore, by comparing the C_s and C_{2v} structures with the experimental structure it has been concluded that the structure does not pass through a well defined transition state structure; rather, the hydrogen vibrates freely between the two oxygen atoms and can be considered to sit in an effective single well potential of asymmetric shape.

Acknowledgment. We thank the Institute Laue-Langevin for the allocation of neutron beam time and Dr. B. B. Iversen, University of Aarhus, for the gift of the crystal. G.K.H.M. and T.M.N. thank the University of Aarhus for financial support.

Supporting Information Available: Experimental results as a PRINTCIF file, Cartesian coordinates and bond lengths from ab initio calculations and the discussion of the CAS results. This material is available free of charge via the Internet at http://pubs.acs.org.

References and Notes

(1) Jeffrey, G. A. *An Introduction to Hydrogen Bonding;* Oxford University Press: Oxford, 1997.

(2) Hibbert, F.; Emsley, J. *Adv. Phys. Org. Chem.* **1990**, *26*, 255−379.

(3) (a) Benoit, M.; Marx, D.; Parrinello, M. *Nature* **1998**, *392*, 258−261. (b) Loubeyre, P.; LeToullec, R.; Wolanin, E.; Hanfland; M.; Hausermann, D. *Nature* **1998**, *397*, 503−506.

(4) Arguments have appeared both for and against the involvement of short hydrogen bonding in enzymatic reaction mechanisms: (a) Cleland, W. W. *Biochemistry* **1992**, *31*, 317−319. (b) Cleland, W. W.; Krevoy, M. M. *Science* **1994**, *264*, 1887−1890. (c) Frey, P. A.; Whitt, S. A.; Tobin, J. B. *Science* **1994**, *264*, 1927−1930. (d) Warshal, A.; Papazyan, A.; Kollman, P. A. *Science* **1995**, *269*, 102−104. (e) Cleland, W. W.; Kreevoy, M. M.; Frey, P. A. *Science* **1995**, *269*, 104−106.

(5) Lundquist, T.; Rice, J.; Hodge, C. N.; Basarab, G. S.; Pierce, J.; Lindquist, Y. *Structure* **1994**, *2*, 937.

(6) Madsen, G. K. H.; Iversen, B. B.; Larsen, F. K.; Kapon, M.; Reisner, G. M.; Herbstein, F. H. *J. Am. Chem. Soc.* **1998**, *120*, 10040−10045.

(7) Emsley, J. *Struct. Bond. (Berlin)* **1984**, *57*, 147−191.

(8) (a) Gilli, G.; Bellucci, F.; Ferretti, V.; Bertolasi, V. *J. Am. Chem. Soc.* **1989**, *111*, 1023−1028. (b) Gilli, P.; Ferretti, V.; Bertolasi, V.; Gilli, G. *Advances in Molecular Structure Research*; Hargittai, M., Hargittai, I., Eds.; JAI Press: Greenwich, CT, 1996; Vol. 2, pp 67−102.

(9) Herbstein, F. H.; Kapon, M.; Reisner, G. M.; Lehmannn, M. S.; Kress, R. B.; Wilson, R. B.; Shiau, W. I.; Duesler, E. N.; Paul, I. C.; Curtin, D. Y. *Proc. R. Soc. London* **1985**, *399*, 295−319.

(10) Simonsen, O.; Thorup, N. *Acta Crystallogr. Sect. B.* **1979**, *35*, 432−435.

(11) Wilkinson, C.; Khamis, H. W.; Stansfield R. F. D.; McIntyre, G. J. *J. Appl. Cryst.* **1988**, *21*, 471−478.

(12) Koritsanszky, T.; Howard, S.; Mallinson, P. R.; Su, Z.; Richter, T.; Hansen, N. K.; *XD, a computer program package for multipole refinement and analysis of charge densities from diffraction data*; Institute of Crystallography, Freie Universität, Berlin, 1995.

(13) Jeffrey, G. A.; Ruble, J. R.; McMullen, R. K.; Pople, J. A. *Proc. R. Soc. London Sect A.* **1987**, *414*, 47−57.

(14) Busing, W. R.; Levy, H. A. *Acta Crystallogr.* **1964**, *17*, 142−146.

(15) Johnson, C. K. In *Thermal Neutron Diffraction;* Willis, B. T. M., Ed.; Oxford University Press: Oxford, 1970.

(16) Johnson, C. K.; Levy, H. A. *International Tables fr X-ray Crystallography*; Kynoch Press: Birmingham, 1974; Vol IV, pp 311−336.

(17) Kuhs, W. F. *Acta Crystallogr. Sect. A* **1992**, *48*, 80−98.

(18) Hirshfeld, F. L. *Acta Crystallogr. Sect. A.* **1976**, *32*, 239−244.

(19) Burnett, M. N.; Johnson, C. K. *ORTEPIII*; Oak Ridge National Laboratory: Tennessee, 1996.

(20) Frisch, M. J.; Trucks, G. W.; Schlegel, H. B.; Gill, P. M. W.; Johnson, B. G.; Robb, M. A.; Cheeseman, J. R.; Keith, T.; Petersson, G. A.; Montgomery, J. A.; Raghavachari, K.; Al-Laham, M. A.; Zakrzewski, V. G.; Ortiz, J. V.; Foresman, J. B.; Cioslowski, J.; Stefanov, B. B.; Nanayakkara, A.; Challacombe, M.; Peng, C. Y.; Ayala, P. Y.; Chen, W.; Wong, M. W.; Andres, J. L.; Replogle, E. S.; Gomperts, R.; Martin, R. L.; Fox, D. J.; Binkley, J. S.; Defrees, D. J.; Baker, J.; Stewart, J. P.; Head-Gordon, M.; Gonzalez, C.; Pople, J. A. *Gaussian 94, Revision E.2.* Gaussian Inc.: Pittsburgh PA, 1995.

(21) Becke, A. D. *J. Chem. Phys.* **1993**, *98*, 5648−5652.

(22) Lee, C.; Yang, W.; Parr, R. G. *Phys. Rev. B* **1988**, *37*, 785−789.

(23) Dunning, T. H., Jr. *J. Chem. Phys.* **1989**, *90*, 1007−1023.

(24) Allen, F. H.; Kennard, O.; Watson, D. G.; Brammer, L.; Orpen, A. G.; Taylor, R. In *International Tables of Crystallography*; Kluwer Academic Publishers: Dordrecht, 1992; Vol. C, pp 685−706.

(25) Takusagawa, F.; Koetzle, T. F. *Acta Crystallogr. Sect B.* **1979**, *35*, 2126−2135.

(26) Flensburg, C.; Larsen, S.; Stewart, R. F. *J. Phys. Chem.* **1995**, *99*, 10130−10141.

(27) Madsen, D.; Flensburg, C.; Larsen, S. *J. Phys. Chem. A* **1998**, *102*, 2177−2188.

(28) Wozniak, K.; Wilson, C. C.; Knight, K. S.; Jones, W.; Grech, E. *Acta Crystallogr. Sect. B* **1996**, *52*, 691−696.

(29) Gilli, P.; Bertolasi, V.; Ferretti, V.; Gilli, G. *J. Am. Chem. Soc.* **1994**, *116*, 909−915.

(30) Jones, R. D. G. *Acta Crystallogr. Sect. B* **1976**, *32*, 2133−2136.

(31) Frisch, M. J.; Scheiner, A. C.; Schaefer, H. F., III; Binkley, J. S. *J. Chem. Phys.* **1985**, *82*, 4194−4198.

(32) Helgaker, T.; Gauss, J.; Jørgensen, P.; Olsen, J. *J. Chem. Phys.* **1997**, *106*, 6430−6440.

(33) Oliphant, N.; Bartlett, R. J. *J. Chem. Phys.* **1994**, *100*, 6550−6561.

(34) Barone, V.; Adamo, C. *J. Chem. Phys.* **1996**, *105*, 11007−11018.

(35) Wolf, K.; Mikenda, W.; Nusterer, E.; Schwarz, K.; Ulbricht, C. *Chem. Eur. J.* **1998**, 1418−1427.